Platinum/Mesoporous WO_3 as a Carbon-Free Electrocatalyst with Enhanced Electrochemical Activity for Methanol Oxidation

Xiangzhi Cui, Jianlin Shi,* Hangrong Chen, Lingxia Zhang, Limin Guo, Jianhua Gao, and Jingbo Li

State Key Laboratory of High Performance Ceramics and Superfine Microstructure, Shanghai Institute of Ceramics, Chinese Academy of Sciences, 1295 Dingxi Road, Shanghai 200050, China

Received: April 23, 2008; Revised Manuscript Received: July 27, 2008

A new type of carbon-free electrode catalyst, Pt/mesoporous WO_3 composite, has been prepared and its electrochemical activity for methanol oxidation has been investigated. The mesoporous tungsten trioxide support was synthesized by a replicating route and the mesoporous composties with Pt loaded were characterized by using X-ray diffraction (XRD), nitrogen sorption, field emission scanning electron microscopy (FE-SEM), transmission electron microscopy (TEM) and energy-dispersive X-ray spectroscopy (EDS) techniques. Cyclic voltammetry (CV), line scan voltammetry (LSV) and chronoamperometry (CA) were adopted to characterize the electrochemical activities of the composites. The mesoporous WO_3 showed high surface area, ordered pore structure, and nanosized wall thickness of about 6−7 nm. When a certain amount of Pt nanoparticles were dispersed in the pore structure of mesoporous WO_3, the resultant mesostructured Pt/WO_3 composites exhibit high electro-catalytic activity toward methanol oxidation. The overall electro-catalytic activities of 20 wt % Pt/WO_3 composites are significantly higher than that of commercial 20 wt % Pt/C catalyst and are comparable to the 20 wt % PtRu/C catalyst in the potential region of 0.5−0.7 V. The enhanced electro-catalytic activity is attributed to be resulted from the assistant catalytic effect and the mesoporous structure of WO_3 supports.

Introduction

Mesoporous materials with ordered pore structures and high surface areas are technologically important for a variety of applications such as in heterogeneous catalysis, adsorption, chemical sensing, electrodes, transportation/storage of fluids and gases, and also in some biological areas.[1−5] In recent years, more and more attention has been paid to the fabrication of novel mesostructured materials prepared by replicating route in which ordered mesoporous silica is employed as a hard template because of its special characters of uniform mesopores, high surface area and large pore volume. The mesoporous transition metal oxides synthesized by this method are highly crystalline and hierarchically ordered on a meso-scale as well as on an atom-scale, and these mesoporous materials also show good structure/thermal stability and many novel properties, which may display potential application prospects in many fields. In our group, Shen et al.[6,7] reported that mesoporous RuO_2 can make the oxidation of CO take place at a very low temperature, and CuO_2-loaded mesoporous CeO_2 composite also shows high catalytic activity toward CO oxidation.

Direct methanol fuel cell (DMFC) has attracted much attention as portable energy source due to its high specific energy at low operating temperature and the ease of handling clean liquid fuel.[8] Unfortunately, some critical technical drawbacks, however, must be solved before it can be commercially applied, which includes the slow oxidation kinetics of methanol, platinum catalyst "poisoning" by CO and the low efficiency of the main component membrane electrode assembly (MEA). Development of novel and effective anode catalysts for methanol oxidation is one of the possible approaches to settle the problems mentioned above. The most widely used anode catalysts are mainly platinum based electro-catalysts which has been extensively studied in fuel cells and is still an important subject of interest.[9−11] Recently, a number of new catalysts, such as binary,[12−14] ternary[15,16] and even quaternary[17,18] metal catalysts, have been developed to increase the methanol electro-oxidation activity. Among them Pt−Ru alloys catalyst is the most active catalysts for methanol oxidation[19−22] and prepared in various methods.[23−27] This improvement of catalytic activity compared to pure platinum can be attributed to a bifunctional mechanism between Pt and Ru, which can reduce the poisoning intermediate CO oxide effectively.[28−31] These catalysts are mostly dispersed on conductive support such as carbon black to achieve high dispersion of the catalysts. Unfortunately, this carbon support cannot prevent the electrode from being poisoned by CO, and meanwhile, the high using amount of metal Pt and Ru is undesirable for its commercial applications. Therefore, in addition to the development of catalysts themselves, recently there also have been great attention for new materials as supports to improve catalytic performance of methanol oxidation.

Tungsten trioxide is an important rare earth oxide, and it has been reported that tungsten oxide has special electrochemical property and may be used as catalysts in fuel cells. This material is known to be able to form a hydrogen tungsten bronze (H_xWO_3) compound in acid solution which is nonstoichiometric and electro-conductive, and this compound can facilitate the dehydrogenation during the reaction of methanol oxidation.[32,33] Pt−WO_3 supported on active carbon have ever been studied as active catalyst for the electro-oxidation of methanol.[34] However, there is no report about the direct loading of Pt particles on mesoporous tungsten oxide to be used as an electrode catalyst. In this report, we take the advantages of the mesoporous structure and the electrochemical merits of tungsten trioxide to

* Corresponding author. Telephone: 86-21-52412714. Fax: 86-21-52413122. E-mail: jlshi@sunm.shcnc.ac.cn.

10.1021/jp803565k CCC: $40.75
Published on Web 08/28/2008

synthesize a carbon-free catalyst, Pt loaded on mesoporous WO_3, by a template replicating method, and this kind of mesostructured catalysts show high electrochemical catalytic activity for methanol oxidation.

Experimental Section

The parent mesoporous silica with cubic *Ia3d* symmetry (designated as KIT-6) was synthesized according to the published procedure using triblock copolymer Pluronic P_{123} ($EO_{20}PO_{70}EO_{20}$) as template by adding *n*-butanol in an acidic aqueous solution.[35]

The mesoporous WO_3 support materials were prepared using as-prepared KIT-6 as hard template and 12-phosphotungstic acid (PW_{12}) as tungsten source, followed by the removal of the hard template using 2 M HF solution. Typically, 1.2 g of 12-phosphotungstic acid was dissolved in 20 mL of ethanol, and this solution was incorporated into 0.8 g of as-prepared KIT-6 by an incipient wetness impregnation technique. After the ethanol evaporation at 313 K, the composite was calcined at 773 K for 3 h to give a decomposition product of tungsten trioxide inside the silica template. The silica template was removed with 2 M HF solution under the stirring for 6 h.This template-free WO_3 was collected by centrifugation, washed with enough distilled water and named as m-WO_3.

Then 0.3 g of as-prepared m-WO_3 powder was dispersed ultrasonically for 15 min in distilled water, and H_2PtCl_6 solution (9.4 mg/mL Pt) was added into the slurry under stirring. After that, excess 0.5 M sodium borohydride solution was dropped slowly in the homogeneous slurry at 298 K, and the reaction was continuous for 12 h under stirring. The deposit was collected by centrifugation and dried at 298 K under vacuum overnight. The composite was named as m-5Pt/WO_3, m-10Pt/WO_3, m-15Pt/WO_3 and m-20Pt/WO_3 according to the different loading amounts of Pt.

X-ray diffraction (XRD) patterns of prepared samples were recorded on a Rigaku D/Max-2550V X-ray diffractometer with a Cu-Ka radiation target (40 kV, 40 mA). The N_2 sorption measurement was performed using Micromeritics Tristar 3000 at 77 K, and specific surface area and the pore size distribution were calculated using the Brunauer−Emmett−Teller (BET) and Barrett−Joyner−Halenda (BJH) methods, respectively. Transmittance electron microscopy (TEM) images were obtained on a JEOL 200CX electron microscope operating at 160 kV. Energy-dispersive X-ray spectra (EDS) was collected from an attached Oxford Link ISIS energy-dispersive spectrometer fixed on a JEM-2010 electron microscope operated at 200 kV. Field emission scanning electron microscopy (FE-SEM) was performed on a JEOL JSM-6700F field emission scanning electron microscopy.

Electrochemical measurement was carried out on CHI660A electrochemical workstation with a half-cell equipment. Glassy carbon disk (o.d. = 6 mm) was served as substrate for the catalyst material. Catalyst ink with 5 mg/mL (ethanol:water = 1:1, volume scale), 25 μL of Nafion solution (5%) was dispersed ultrasonically, and 20 μL was transferred onto the glassy carbon substrate yielding a catalyst loading level of 0.35 mg/cm.^{2} The resulting thin catalyst film was obtained after solvent evaporation at 333 K. A solution of 0.5 M CH_3OH + 0.5 M H_2SO_4 was used for methanol electro-oxidation study. The catalysts were characterized by cyclic voltammetry (CV) and line scan voltammetry (LSV) at 298 K with platinum sheet and Ag/AgCl/3 M KCl as the counter and the reference electrodes, respectively. Steady state polarization measurements were recorded point by point in the potentionstatic mode at several rotation rates (1600 rpm), and chronoamperometry (CA) was also adopted to characterize the activity and stability of catalysts for methanol oxidation. Highly pure N_2 was used prior to the measurements to deaerate the electrolyte.

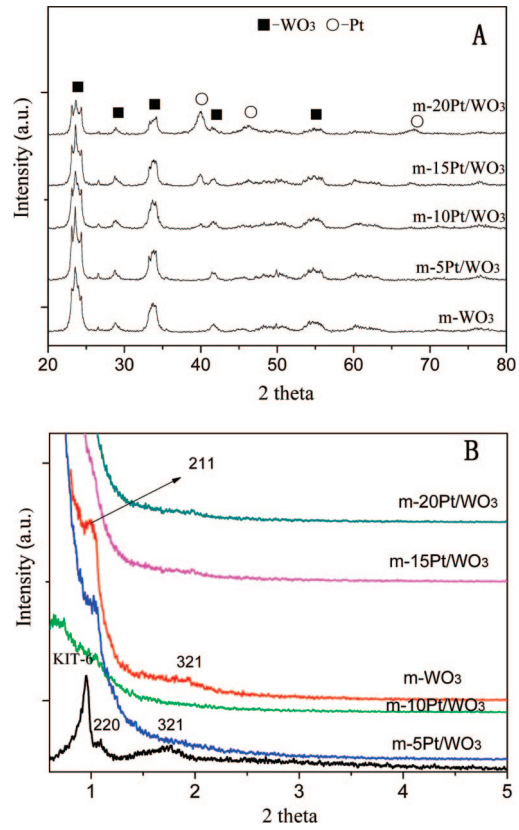

Figure 1. XRD patterns of mesostructured m-Pt/WO_3 composites: (A) high-angle XRD patterns and (B) low-angle XRD patterns.

Results and Discussion

Structural characteristics. Typical XRD patterns for the prepared samples are shown in Figure 1. It can be found that all of the diffraction peaks of template-free m-WO_3 can be indexed to pure monoclinic WO_3 (JCPDS card no. 20−1324), indicating well-crystallized WO_3 framework. After loading with 5 wt % Pt metal, the XRD pattern of m-5PtWO_3 composite does not show apparent presence of metallic platinum because of its low loading amount. With the increase of Pt loading amount, the presence of metallic platinum is clearly revealed by the characteristic diffraction peaks of Pt[111] and [200] planes at 2θ values of 39.8° and 46.2°, respectively (JCPDS 04−0802), and the Pt [220] also appears at 67.4° when loaded with 20 wt % Pt. The peak at $2\theta = 46.2°$ was used to calculate the mean size of Pt nanoparticles using the Debye−Scherer equation.[36] The average crystallite size of Pt and WO_3 was found to be about 6.5nm and 6.2 nm, respectively. According to the low-angle XRD patterns in Figure 1B, template KIT-6 exhibits three well-resolved diffraction peaks in the 2θ range between 0.5 and 3°, which can be indexed as (211), (220) and (321) reflections associated with cubic symmetry (*Ia3d* space group). The tungsten trioxide replica m-WO_3 shows the similar characteristic low angle diffraction peaks as the silica template belonging to the same symmetry with slightly shifted peak position to higher angle, suggesting that the WO_3 product retains the ordered mesoporous structure and inherits the cubic Ia3d symmetry structure of the template. However, only one peak (211) can be seen in the low angle region for the sample

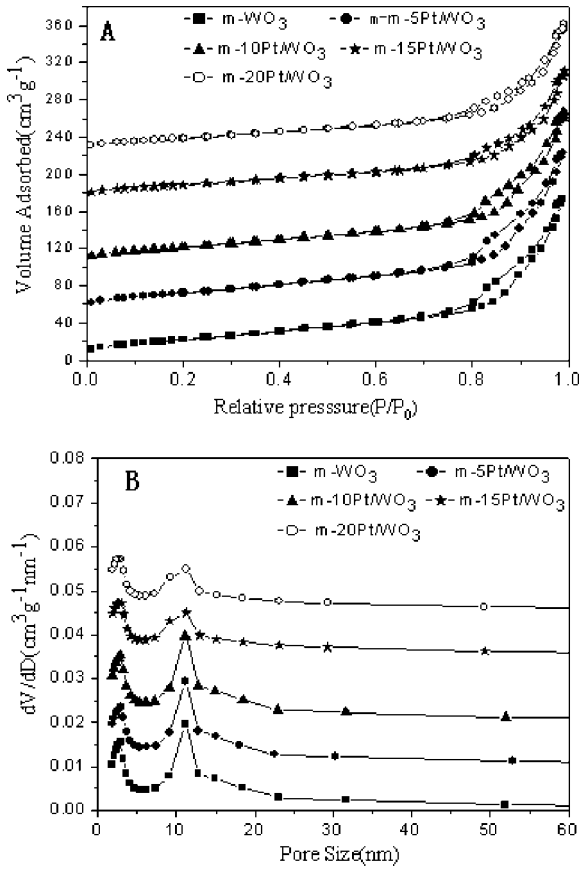

Figure 2. (A) Nitrogen sorption isotherms and (B) the corresponding pore size distributions for mesostructured m-Pt/WO_3 composites.

TABLE 1: Pore Structure Parameters of the m-WO_3 and m-Pt/WO_3 Composites

sample	XRD results /nm	BET surface area /$m^2 \cdot g^{-1}$	BJH pore size /nm	pore volume / $cm^3 \cdot g^{-1}$	thickness of wall[a] /nm
KIT-6c	$d_{211} = 9.519$	820	6.51	1.26	4.5
m-WO_3	$d_{211} = 8.669$	86	8.6	0.12	6.2[b]
m-5Pt/WO_3		80	9.2	0.11	
m-10Pt/WO_3		78	10	0.11	
m-15Pt/WO_3		72	11.4	0.10	
m-20Pt/WO_3		73	12.0	0.10	

[a] Thickness of wall = $2d_{211}/3 \times$ BJH pore size. [b] Denotes the diameter of WO_3 nanorods.

m-5PtWO_3, and it can no longer be detected for samples m-15PtWO_3 and m-20PtWO_3 at increased Pt loading amount, which means that the ordered mesostructure has been destroyed after the loading of Pt.

The nitrogen sorption isotherms of samples have been recorded and shown in Figure 2A. All of the samples show similar isotherm curves with a weak jump at $P/P_0 = 0.3-0.5$ and another jump at $P/P_0 = 0.8-0.9$, which is the characteristic of mesoporous solids. This indicates that the mesostructure of m-PtWO_3 composites have been kept after the incorporation of metal Pt particles. The data of specific surface areas of these samples with the corresponding pore sizes and pore volumes are summarized in Table 1. The BET specific surface area of the prepared mesoporous WO_3 is 86 $m^2 \cdot g^{-1}$, and the wall thickness (diameter of WO_3 nanorods or nanoparticles) is 6.2 nm, close to the pore size of silica template (6.51 nm). The mean pore size of m-WO_3, however, is larger than the wall thickness of the silica template according to the data in Table 1. This is due to the bimodal pore size distributions in the ranges

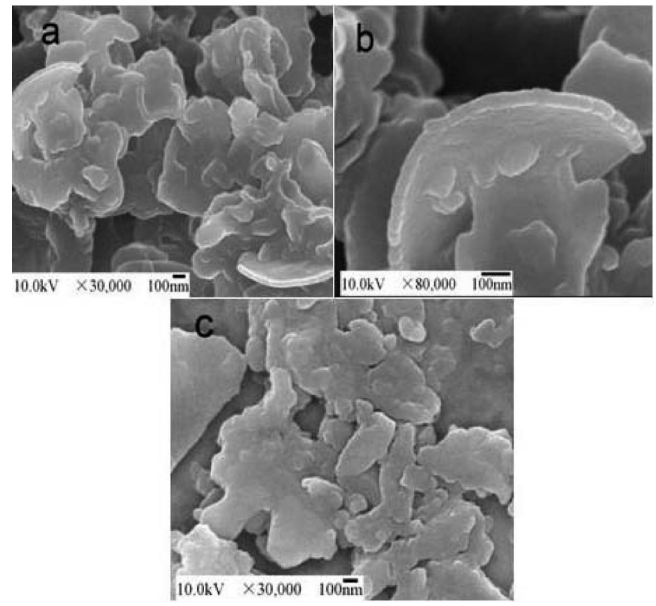

Figure 3. Typical FE-SEM images of the prepared m-WO_3 sample at different magnifications (a, b) and the mesoporous silica template (c).

2−4 nm and 9−12 nm as shown in Figure 2B. The pores of 2−4 nm are produced by the removal of silica wall, and those of 9−12 nm are due to the textural porosity among the particles. The BET specific surface areas and the pore volumes of m-PtWO_3 composites decrease gradually with the increase of Pt loading amount. This is due to the fact that, at the increased Pt loading amount, more Pt nanoparticles were dispersed within the pore channels of the mesoporous WO_3 support, leading to the blocking of the pore channels and the decrease of measured surface areas and pore volumes of the Pt/WO_3 composites. In addition, the pore size distribution become wider with the increase of Pt loading amount (Figure 2B), this is due to the ordering deterioration of the mesoporous structure of the Pt/WO_3 composites when higher amounts of Pt were loaded, as can be found in the low-angle XRD patterns in Figure 1B with no low angle diffraction peaks detected for samples m-15PtWO_3 and m-20PtWO_3.

The representative FE-SEM images of the prepared m-WO_3 can be found in Figure 3, parts a and b. It can be seen that such a material exhibits a curled and flake-like morphology with a flake thickness of about 50 nm. Figure 3c is the typical FE-SEM image of pure mesoporous silica (KIT-6). It could be found that the prepared m-WO_3 has well inherited the flake-like morphology of silica template.

The typical TEM images in Figure 4, parts a and b, show that the m-WO_3 replica possesses well ordered mesoporous framework in the view of (111) and (100) directions of cubic *Ia3d* symmetry, respectively, which is consistent with the mesoporous framework of pure KIT-6 template (Figure 4d). It can be estimated from the TEM image of (100) direction that the diameter of the nanorods for the m-WO_3 framework is about 6−7 nm, which is in accordance with the pore size of the hard template (6.51 nm). This indicates that the WO_3 framework is a good replica of the mesoporous structure of silica template. The Si signal can be hardly detected in the EDS pattern of Figure 4c performed on different domains of the template-free m-WO_3 meaning the complete removal of silica template. The selected area electron diffraction (SAED) pattern (inset in Figure 4b) indicates that the m-WO_3 replica is well crystallized and has a polycrystalline character.

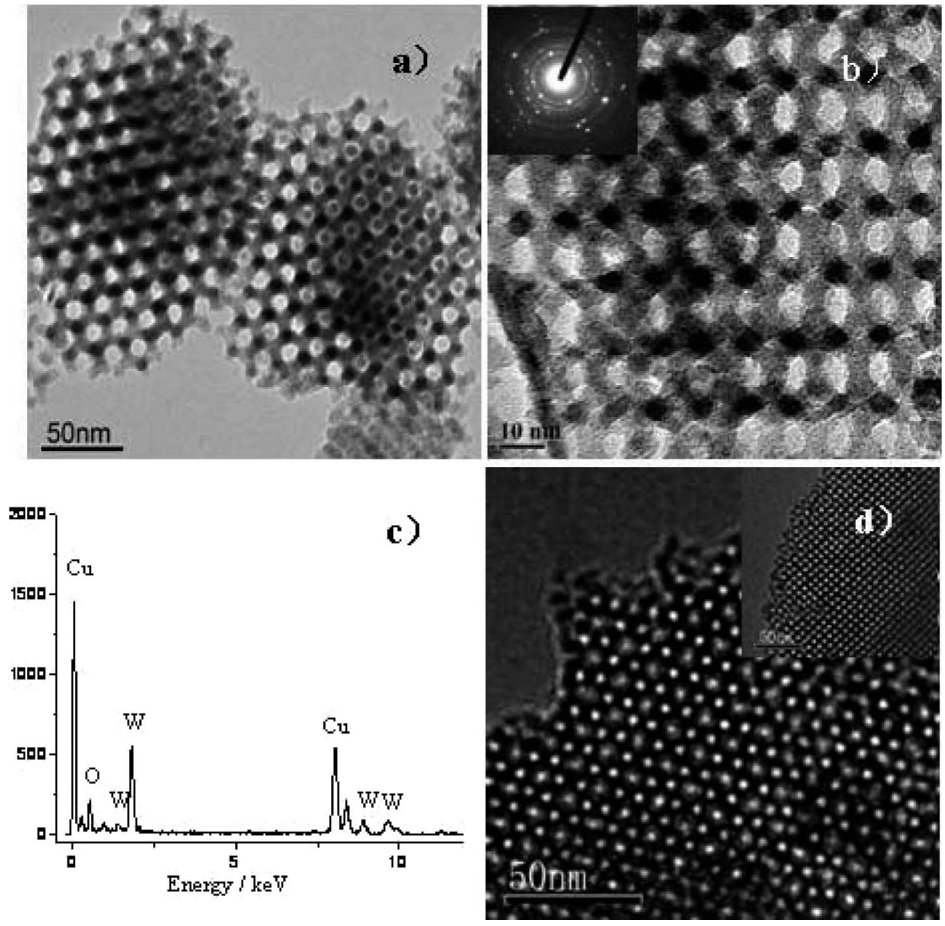

Figure 4. TEM images (a, b) of m-WO_3 in [111] and [100] directions, respectively, with the SAED pattern of m-WO_3 as the inset in part b; EDS pattern of m-WO_3 (c); TEM images of KIT-6 (d) in [111] direction and in [100] direction (inset in d).

TEM images of composites m-15Pt/WO_3 and m-20Pt/WO_3, in Figure 5, parts a and b, respectively, show that Pt nanoparticles of darker dots are dispersed well in the pore structure of mesoporous WO_3. No very large metal particles/aggregates can be found, however, some metal Pt nanoparticles may exist outside of the mesopores of WO_3 when the Pt loading amount comes up to 20 wt % as shown in the selected area in Figure 5b. Small Pt nanoparticles can be found existing within the pores of the mesoporous WO_3 support in a larger magnification image of Figure 5c. The high-resolution TEM in Figure 5d shows two kinds of crystal lattice stripes. The smaller one of $d = 0.23$nm belongs to the Pt metal ($d = 0.226$nm, JCPDS 04−0802) and another one of d=0.27nm should be WO_3 according to JCPDS card no. 20−1324, which is an additional evidence to prove the Pt particles existing in the pores of the support. A more direct evidence of Pt nanoparticles dispersed in the WO_3 matrix is the clear Pt signals easily detected by EDS in Figure 5e obtained on these composites.

Electrochemical Properties for Methanol Oxidation. The electro-catalytic curves of methanol oxidation on mesostructured WO_3 and m-Pt/WO_3 composites are shown in Figure 6A, and the corresponding electrochemical parameters are listed in Table 2. The pure m-WO_3 without Pt displays no electrochemcial activity. By contrast, the mesostructrued Pt/WO_3 composites show high current density for methanol oxidation with a specific activity sequence as following: m-20Pt/WO_3 > m-15Pt/WO_3 > 20 wt % Pt/C > m-10Pt/WO_3 > m-5Pt/WO_3. The electro-catalytic activity of m-20Pt/WO_3 is 55% higher than that of the commercial catalyst 20 wt % Pt/C. The sample m-10Pt/WO_3 shows the highest mass activity (706 mA·mg-Pt^{-1}) among all the catalysts, which is 80% higher than that of the 20 wt % Pt/C (383 mA·mg-Pt^{-1}) from the data in Table 2. These indicate that the catalysts of Pt supported on mesoporous WO_3 have high electro-catalytic activity toward methanol oxidation.

It can also be seen, in Figure 6A, that the peak potentials in positive scan on m-5Pt/WO_3 and m-10Pt/WO_3 are lower than that of 20 wt % Pt/C catalyst, which means that methanol oxidation on the two samples can take place at a lower potential. While the peak potentials of m-15Pt/WO_3 and m-20Pt/WO_3 move to higher value (0.72 V) as compared to 20 wt % Pt/C (0.7 V) suggesting that the methanol oxidation need a little higher potential on the m-Pt/WO_3 composites of higher Pt loading amount. The enhanced electrochemical activity of m-Pt/WO_3 composites toward methanol oxidation can be attributed to the assistant catalytic effect and the mesoporous structure of mesoporous WO_3 support as discussed below.

Many researchers have studied the electro-catalytic properties and electrochemical characteristic of Pt-tungsten oxide in acidic electrolyte. It has been reported that tungsten oxide could form two stable hydrogen tungsten bronzes, $H_{0.18}WO_3$ and $H_{0.35}WO_3$, and substoichiometric oxides, WO_{3-y}, by reaction with hydrogen in the electrolyte. [37]

$$WO_3 + xH^+ + xe^- \rightarrow H_xWO_3 \quad (0 < x < 1) \qquad (1)$$

$$WO_3 + 2yH^+ + 2ye^- \rightarrow WO_3 + yH_2O \quad (0 < y < 1) \qquad (2)$$

Methanol oxidation is a complicated chemical reaction. As reported by Laborde, H. et al. [38] methanol molecules (CH_3OH)

are first absorbed on Pt and disassembled as intermediate $Pt-(CHO)_{ads}$, which reacted with $Pt-(OH)_{ads}$ to give CO_2 and H^+. The reaction mechanism is proposed as the following chemical reactions, as put forward previously by several researchers in literatures.[39−41]

Normal Pt catalysis mechanism:

$$Pt + H_2O \rightarrow Pt-(OH)_{ads} + H^+ + e^- \quad (3)$$

$$Pt-(CHO)_{ads} + Pt-(OH)_{ads} \rightarrow 2Pt + CO_2 + 2H^+ + 2e^- \quad (4)$$

Bronze route mechanism:

$$Pt-(CHO)_{ads} + Pt-(OH)_{ads} + WO_3 \rightarrow 2Pt + CO_2 + H_xWO_3 \quad (5)$$

$$H_xWO_3 \rightarrow WO_3 + xH^+ + xe^- \quad (6)$$

Following the reactions of (5) and (6), finally methanol molecules are oxidized following the equation:[42]

$$CH_3OH + H_2O \rightarrow CO_2 + 6H^+_{aq} + 6e^- \quad E^\circ = 0.03\ V \quad (7)$$

For the composite catalyst of Pt supported on mesoporous WO_3, WO_3 can form a hydrogen tungsten bronzes compound ($HxWO_3$) in acidic electrolyte and this tungsten bronzes compound can make the dehydrogenation of methanol molecules adsorbed on Pt surface more effective,[33] since the spillover of hydrogen onto the surface of hydrogen tungsten bronze can free these Pt sites for further chemisorption of methanol molecules.[43]

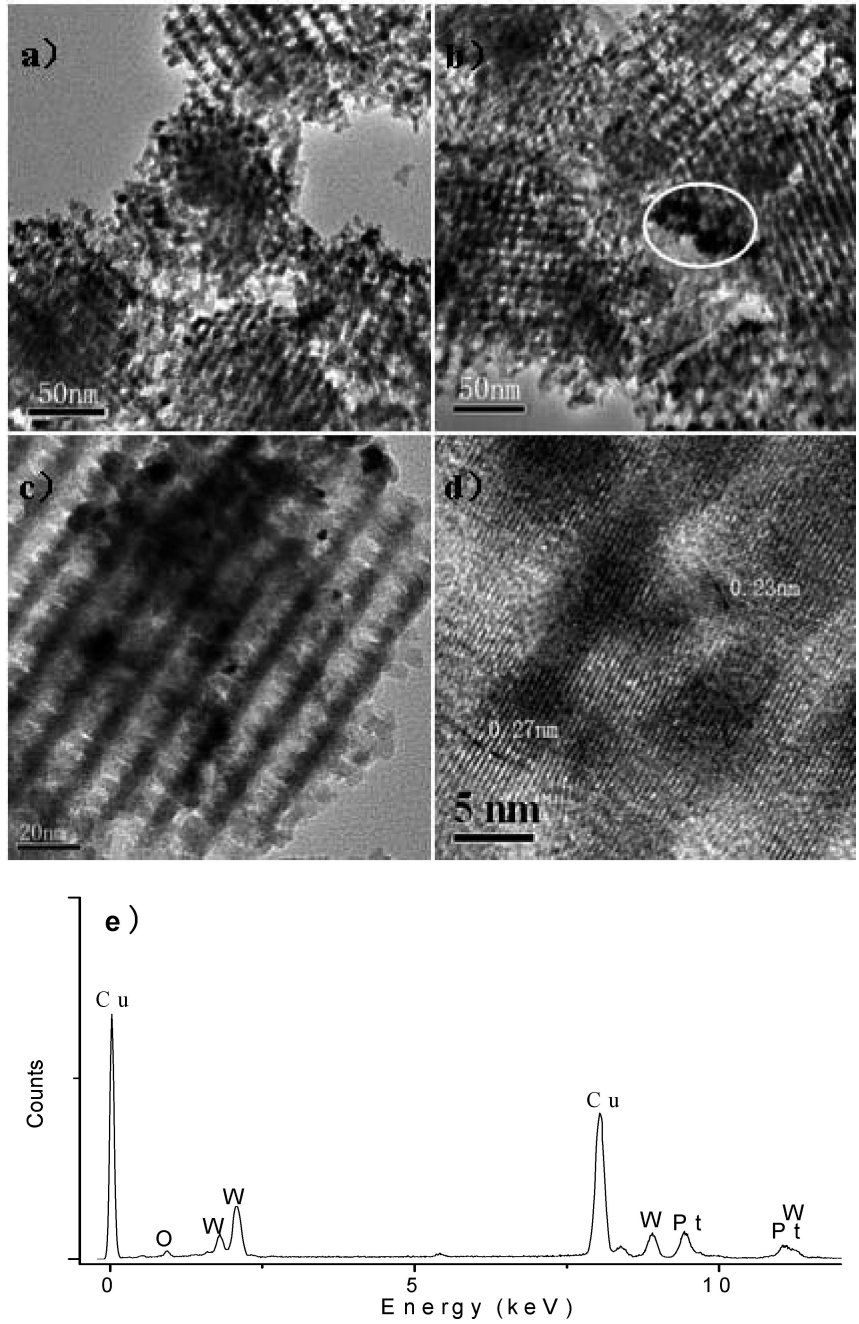

Figure 5. TEM images of mesostructured m-15Pt/WO_3 (a, c), m-20Pt/WO_3 (b); high-resolution TEM image (d) and EDS pattern (e) of m-15Pt/WO_3.

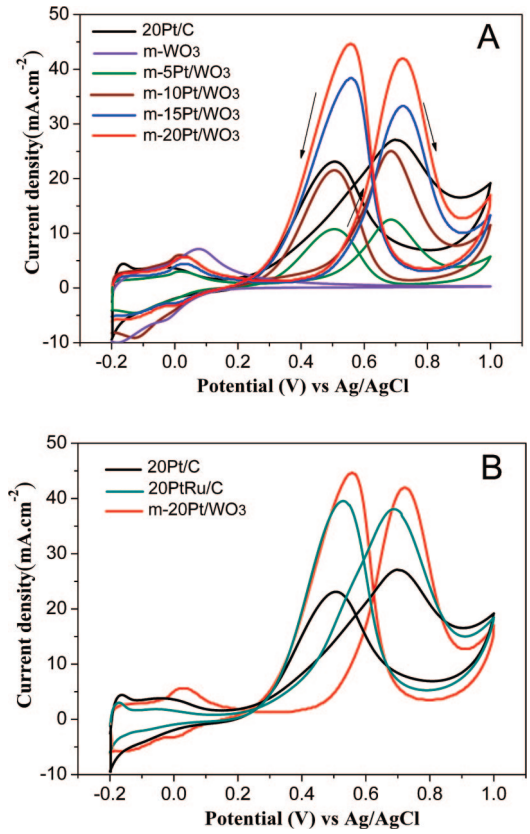

Figure 6. Cyclic voltammetry curves of samples for methanol oxidation in 0.5 M CH_3OH + 0.5 M H_2SO_4 electrolyte, with a scan rate of 50 mV s^{-1} at 298 K (the arrows indicate the direction of scanning).

TABLE 2: Electro-Catalytic Activity of Mesostructured m-WO_3 and m-Pt/WO_3 Composites for Methanol Oxidation in 0.5 M H_2SO_4 + 0.5 M CH_3OH Solution

catalyst	specific activity[a] at 0.7V/ mA cm^{-2}	mass activity[b] at 0.7V/ mA mg-Pt^{-1}	potential of max current[c] /V	difference potential[d] /mV
m-WO_3	0	0		
m-5Pt/WO_3	12	678	0.69	175
m-10Pt/WO_3	25	706	0.70	175
m-15Pt/WO_3	32.3	609	0.72	153
m-20Pt/WO_3	41.9	592	0.72	152
20 wt % Pt/C	27.1	383	0.70	196

[a] Intrinsic activity of the Pt site, has been normalized to the electrochemical active surface areas. [b] Intrinsic activity of the Pt site, has been normalized to the mass of Pt. [c] Potential of maximum methanol oxidation current in positive scan. [d] Potential difference between two current peaks of methanol oxidation in positive scan and negative scan.

In addition, the oxophilic nature of the oxide also helps in removing the adsorbed intermediates during the methanol oxidation.[44]

From the chemical reaction above, it may be true that mesoporous WO_3 acts not only as catalyst support, but also assists in the electro-catalysis of Pt in methanol oxidation by forming an intermediate compound of hydrogen tungsten bronze. Besides, another important reason is the high surface area and unique mesoporous structure of WO_3 support, which favors the formation of hydrogen tungsten bronzes, and meanwhile provide more active sites for the chemisorption and oxidation of methanol molecules than conventional Pt/C catalyst and thus accelerate the process of the electrochemical reactions.

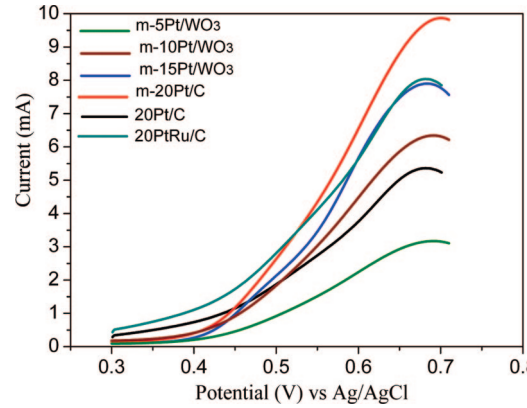

Figure 7. Line scan voltammetry curves of samples for methanol oxidation with a scan rate of 10 mV s^{-1} at 298 K.

It can also be found in Table 2 that the differences between the potentials for the forward and the backward sweeps are significantly smaller on m-Pt/WO_3 composites than that on commercial catalyst 20 wt % Pt/C (196mV), which means that the mesostructured m-Pt/WO_3 catalyst has better tolerance toward CO poisoning.[45]

The electrochemical activity for methanol oxidation of the commercial 20 wt % PtRu/C catalyst was also measured for comparison, and the result is shown in Figure 6B. It could be found that the peak currents of m-20Pt/WO_3 are comparable to and even higher than that of 20 wt % PtRu/C, though PtRu/C has been reported to be a much better catalyst for methanol oxidation than Pt/C.[46]

Figure 7 is the line scan voltammetry (LSV) curves of catalysts from 0.3−0.7 V with a scan rate of 10mV/s. It can be seen that the onset potentials for methanol oxidation of all m-Pt/WO_3 catalysts are very close to each other and are higher than that on 20 wt % Pt/C and 20 wt % PtRu/C catalysts. This difference can be related to the different electric conductivity between carbon and the current WO_3 supports. Among all the m-Pt/WO_3 catalysts, the current of m-20Pt/WO_3 increases at the fastest rate. It should be noted that the electro-catalytic activity of m-20Pt/WO_3 is significantly higher than that of 20 wt % Pt/C at above 0.45 V and higher than that of 20 wt % PtRu/C at above 0.52 V, respectively, though the onset potential of m-20Pt/WO_3 for methanol oxidation is higher than those of the commercial catalysts. It is also noted, however, that the current output of m-20Pt/WO_3 toward methanol oxidation at low potential region, typically under 0.5 V, is lower than that of 20 wt % PtRu/C. Such a higher activity of 20 wt % PtRu/C catalyst at the low potential region can be attributed to the much better catalytic activity of PtRu metal alloy than single metal Pt, [47] and the better electric conductivity of carbon than WO_3.

In order to further study the electrochemical properties on methanol oxidation, the chronoamperometry was employed and the testing results are shown in Figure 8. The activity and stability of catalysts at 0.65 V follow the sequence: m-20Pt/WO_3 > m-15Pt/WO_3 > m-10Pt/WO_3 ≈ 20 wt % Pt/C > m-5Pt/WO_3 (Figure 8A). The current values of m-10Pt/WO_3 and 20 wt % Pt/C at the end of the test are very close to each other, and this result is different from CV tests, where the peak current of 20 wt % Pt/C is higher than that of m-10Pt/WO_3. The relatively lower electro-catalytic activity of methanol oxidation on 20 wt % Pt/C catalyst is probably resulted from the CO "poisoning" of Pt. For comparison, 20 wt % PtRu/C catalyst was also measured. It is clear that the current output of m-20Pt/WO_3 is higher than 20 wt % PtRu/C at the end of the test, and

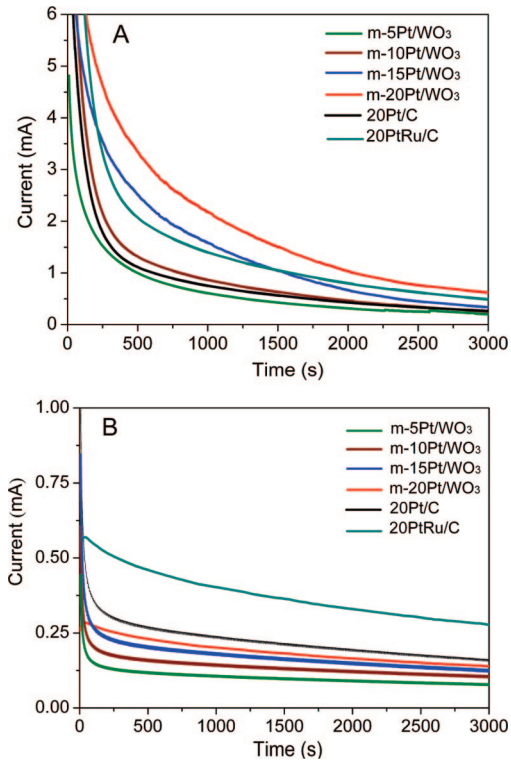

Figure 8. Chronoamperometry curves of catalysts for methanol oxidation measured at 0.65 (A) and 0.32 V (B), 298 K.

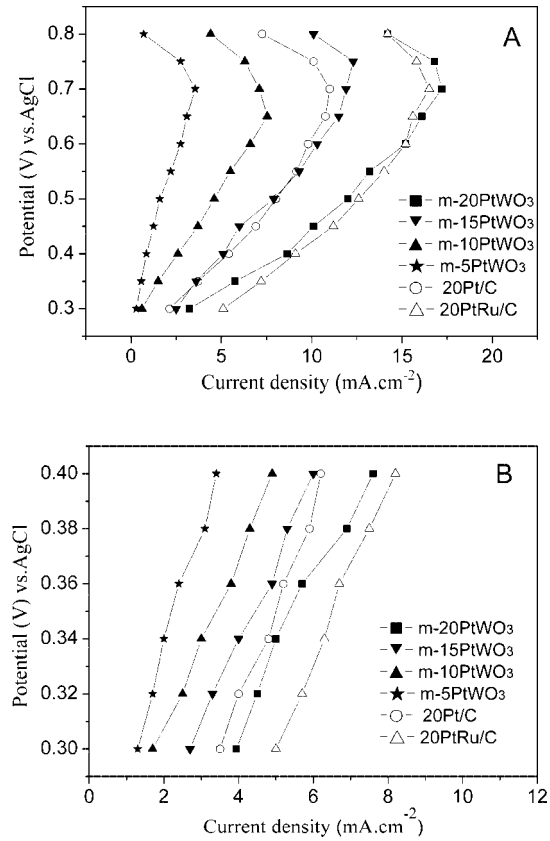

Figure 9. Polarization curves of different catalysts for methanol oxidation (A) and more detailed data in the potential region of 0.3−0.4V (B) at 298 K.

both of them, as expected, are much higher than 20 wt % Pt/C. However, at the low potential of 0.32V (Figure 8B), 20 wt % PtRu/C shows considerably higher current than that of m-Pt/WO_3 composites and 20 wt % Pt/C, meaning that PtRu/C has higher electro-catalytic activity on methanol oxidation at low potentials. This is consistent with the LSV results (Figure 7). As the chronoamperometry test is close to the practical single cell operation, so we believe that the chronoamperometry test result can represent the activity and stability of catalysts more accurately. In the following chronoamperometry tests, the current is kept constant and the methanol is electro-oxidized continuously, thus the reaction is exactly the same as that under DMFC operating condition.

Figure 9A gives the steady-state polarization curves for methanol oxidation on catalysts in the potential range of 0.3−0.8 V, and the more detailed polarization data in the low potential region (0.3−0.4 V) are also presented in Figure 9B. It can be seen that the electro-catalytic activity of all samples for methanol oxidation increases with the increaseof potential and Pt loading amount, while the currents decrease when the potential is higher than 0.75 V, which is due to the activity loss (polarization) of catalysts at high potentials. These results are consistent with the CV tests (Figure 6). The commercial catalyst 20 wt % PtRu/C shows rather close electro-catalytic activity to m-20Pt/WO_3 for methanol oxidation at 0.4V and above, though the former exhibits a little higher current density in the low potential region (Figure 9B). Polarization curves of methanol oxidation has been reported to be in agreement with the result of single cell,[48] so the above results indicate that the overall catalytic activity of m-20Pt/WO_3 on methanol oxidation is considerably higher than that of 20 wt % Pt/C catalyst and is close to or even slightly higher than that of 20 wt % PtRu/C in high potential region (0.5−0.7 V), though it is a little lower than that of 20 wt % PtRu/C in low potential region (0.3−0.4 V).

Conclusion

Mesoporous WO_3 with ordered pore structure has been synthesized by a template replicating route and characterized. When the mesoporous WO_3 being used as catalyst support and loaded with metal Pt nanoparticles, this carbon-free mesostructrued Pt/WO_3 composites show high electro-catalytic activity toward methanol oxidation and good electrochemical stability. The overall activities of 20 wt % Pt/WO_3 composites for methanol oxidation are significantly higher than that of commercial 20 wt % Pt/C catalysts, and it is comparable to or even higher than that of 20 wt % PtRu/C catalyst in potential region of 0.5–0.7 V and lower than 20 wt % PtRu/C in low potential region of 0.3−0.4 V. The enhanced electro-catalytic activity of methanol oxidation on m-Pt/WO_3 composites is attributed to the assistant catalytic effect and the mesoporous structure of WO_3 support.

Acknowledgment. The authors gratefully acknowledge the financial support from National Natural Science Foundation of China with Contract (20633090), National Fundamental Research Project (2002CB613305), Qiming Star Project of Shanghai with Contract 05QMX1458, and Foundation of Shanghai nanotechnology (0552nm030).

References and Notes

(1) Chen, H. R.; Gu, J. L.; Shi, J. L.; Liu, Z. C.; Gao, J. H.; Ruan, M. L.; Yan, D. S. *Adv. Mater.* **2005**, *17*, 2010.
(2) Cai, X. H.; Zhu, G. S.; Zhang, W. W.; Zhao, H. Y.; Wang, C.; Qiu, S. L.; Wei, Y. *Eur. J. Inorg. Chem.* **2006**, 3641.
(3) Zhao, D. Y.; Yang, P. D.; Chmelka, B. F.; Stucky, G. D. *Chem. Mater.* **1999**, *11*, 1174.
(4) Dong, A. G.; Wang, Y. J.; Tang, Y.; Ren, N.; Zhang, Y. H.; Yue, Y. H.; Gao, Z. *Adv. Mater.* **2002**, *14*, 926.

(5) Lee, Y. J.; Lee, J. S.; Park, Y. S.; Yoon, K. B. *Adv. Mater.* **2001**, *13*, 1295.

(6) Shen, W. H.; Shi, J. L.; Chen, H. R.; Gu, J. L.; Zhu, Y. F.; Dong, X. P. *Chem. Lett.* **2005**, *34*, 390.

(7) Shen, W. H.; Dong, X. P.; Zhu, Y. F.; Chen, H. R.; Shi, J. L *Micropor. Mesopor. Mat.* **2005**, *85*, 157.

(8) Winter, M.; Brodd, R. J. *Chem. Rev.* **2004**, *104*, 4245.

(9) Kucernak, A.; Jiang, J. *Chem. Eng. J.* **2003**, *93*, 81.

(10) Umeda, M.; Kokubo, M.; Mohamedi, M.; Uchida, I. *Electrochim. Acta* **2003**, *48*, 1367.

(11) Tripkovic, A. V.; Popovic, K. D.; Grgur, B. N.; Blinzanac, B.; Ross, P. N.; Markovic, N. M. *Electrochim. Acta* **2002**, *47*, 3707.

(12) Beden, B.; Kadirgan, F.; Lamy, C.; Leger, J. M. *J. Electroanal. Chem.* **1981**, *127*, 75.

(13) Arico, A. S.; Kim, H.; Shukla, A. K.; Ravikumar, M. K.; Antonucci, V.; Giordano, N. *Electrochim. Acta* **1994**, *39*, 691.

(14) Saffarian, H. M.; Srinivasan, R.; Chu, D.; Gilman, S. *Electrochim. Acta* **1998**, *44*, 1447.

(15) Shukla, A. K.; Ravikumar, M. K.; S.Arico, A.; Candiano, G.; Antonucci, V.; Giordano, N.; Hamlet, A. *J. Appl. Electrochem.* **1995**, *25*, 528.

(16) Shen, P. K.; Tseung, A. C. *J. Electrochem. Soc.* **1994**, *141*, 3082.

(17) Reddington, E.; Sapienza, A.; Gurau, B.; Viswanathan, R.; Sarangpani, S.; Smokin, E. S.; Mallouk, T. E. *Science.* **1998**, *280*, 1735.

(18) Arico, A. S.; Poltarzewski, Z.; Kim, H.; Morana, A.; Giordano, N.; Antonucci, V. *J. Power Sources* **1995**, *55*, 159.

(19) Gasteiger, H. A.; Markovic, N.; Ross, P. N.; Cairns, E. J. *J. Electrochem. Soc.* **1994**, *141*, 1795.

(20) Anderson, A. B.; Grantscharora, E.; Shiller, P. *J. Electrochem. Soc.* **1995**, *142*, 1880.

(21) Gasteiger, H. A.; Markovic, N.; Ross, P. N.; Cairns, E. J. *J. Phys. Chem.* **1994**, *98*, 617.

(22) Gasteiger, H. A.; Markovic, N.; Ross, P. N.; Cairns, E. J. *J. Phys. Chem.* **1993**, *97*, 12020.

(23) Krausa, M.; Vielstich, W. *J. Electroanal. Chem.* **1994**, *379*, 307.

(24) Arico, A. S.; Poltarzewski, Z.; Kim, H.; Morana, A.; Giordano, N.; Antonucci, V. *J. Power Sources* **1995**, *55*, 159.

(25) Kelley, S. C.; Deluga, G. A.; Smyrl, W. H. *Electrochem. Solid-State Lett.* **2000**, *3*, 407.

(26) Iwasita, T.; Hoster, H.; John-Anacker, A.; Lin, W. F.; Vielstich, W. *Langmuir* **2000**, *16*, 522.

(27) Kardash, D.; Korzeniewski, C.; Markovic, N. *J. Electroanal. Chem.* **2001**, *500*, 518.

(28) Lizcano-Valbuena, W. H.; Paganin, V. A.; Gonzalez, E. R. *Electrochim. Acta* **2002**, *47*, 3715.

(29) Wang, K.; Gasteiger, H. A.; Markovic, N. M.; Ross, P. N. *Electrochim. Acta* **1996**, *41*, 2587.

(30) Ticanelli, E.; Beery, J. G.; Paffett, M. T.; Gottesfeld, S. *J. Electroanal. Chem.* **1989**, *258*, 61.

(31) Iwasita, T. *Electrochim. Acta* **2002**, *47*, 3663.

(32) Kulesza, P. J.; Faulkner, L. R. *J. Electroanal. Chem.* **1989**, *259*, 81.

(33) Tseung, A. C.C.; Chen, K. Y. *Catal. Today.* **1997**, *38*, 439.

(34) Shen, P. K.; Chen, P. K.; Tseung, A. C. C. *J. Chem. Soc., Faraday Trans.* **1994**, *90*, 3089.

(35) Kleitz, F.; Choi, S. H.; Ryoo, R. *Chem. Commun.* **2003**, *35*, 2136.

(36) Warren, B. E. *X-ray Diffraction*; Addison-Wesley: Reading, MA, 1996.

(37) Kulesza, P. J.; Faulkner, L. R. *J. Am. Chem. Soc.* **1988**, *110*, 4905.

(38) Laborde, H.; Leger, T. M.; Lamy, C. *J. Appl. Electrochem.* **1994**, *24*, 219.

(39) Kulesza, P. J.; Faulkner, L. R. *J. Electroanal. Chem.* **1989**, *259*, 81.

(40) Hobbs, B. S.; Tseung, A. C. C. *J. Electrochem. Soc.* **1972**, *119*, 580.

(41) Hobbs, B. S.; Tseung, A. C. C. *J. Electrochem. Soc.* **1973**, *120*, 766.

(42) Shrisudersan, J.; Thomas, F. J.; Sung-Hyeon, B.; Eric, W. M. *J. Phys. Chem. B* **2005**, *109*, 22958.

(43) Hobbs, B. S.; Tseung, A. C.C. *Nature.* **1969**, *222*, 2723.

(44) Tseung, A. C. C.; Chen, K. Y. *Catal. Today* **1997**, *38*, 439.

(45) Rajesh, B.; Thampi, K. R.; Bonard, J. M.; Xanthopoulos, N.; Mathieu, H. J.; Viswanathan, B. *J. Phys. Chem. B* **2003**, *107*, 2701.

(46) Lin, S. D.; Hsiao, T. C.; Chang, J. R.; Lin, A. S. *J. Phys. Chem. B.* **1999**, *103*, 97.

(47) Schmidt, T. J.; Noedke, M.; Gasteiger, H. A. *J. Electrochem. Soc. [J]* **1998**, *145*, 925.

(48) Gotz, M.; Wendt, H. *J. Appl. Electrochem. [J]* **2001**, *31*, 811.

JP803565K